Computer Physics Communications 287 (2023) 108693

Contents lists available at ScienceDirect

Computer Physics Communications

journal homepage: www.elsevier.com/locate/cpc

Exploiting underlying crystal lattice for efficient computation of Coulomb matrix elements in multi-million atoms nanostructures ☆,☆☆

Piotr T. Różański *, Michał Zieliński

Institute of Physics, Faculty of Physics, Astronomy and Informatics, Nicolaus Copernicus University, ul. Grudziądzka 5, 87-100 Toruń, Poland

ARTICLE INFO

Article history:
Received 26 September 2022
Received in revised form 14 January 2023
Accepted 7 February 2023
Available online 17 February 2023

Dataset link: https://github.com/develancer/coulombo-lattice

Keywords:
Quantum dots
Crystal quantum dots
Atomistic calculations
Crystal lattice
Linear scaling
Fast Fourier transform
Dopants in silicon

ABSTRACT

Atomistic modeling of nanostructures often leads to computationally challenging problems involving millions of atoms and tens of thousands of Coulomb matrix elements. In our previous work, we presented a practical solution to this problem, where quasi-linear efficiency, both in time and memory, was obtained by utilizing the fast Fourier transform. Here, we present an updated version of our highly-parallelized computer program, named Coulombo-Lattice, that eliminates the necessity of introducing an auxiliary basis set for the wave-function transfer to the computational grid. Here, we instead exploit the properties of the underlying crystal lattice and run calculations on a regular three-dimensional grid superimposed on the original, lower-symmetry lattice. Due to removal of spurious interactions from other supercells, the resulting Coulomb matrix elements are, up to numerical precision, identical to those obtained by the direct summation $O(N^2)$ method, yet our code maintains $O(N \log N)$ scaling. We illustrate our approach by calculations involving up to 1.7 million integrals, and number of atoms reaching up to 2.8 million, for the problem of dopant charging energy for a single phosphorus dopant embedded in a silicon lattice. Next, to emphasize the broad applicability of our code, we show the results for mixed zinc-blend/wurtzite lattice systems, also known as crystal phase quantum dots.

Program summary

Program Title: Coulombo-Lattice
CPC Library link to program files: https://doi.org/10.17632/jwkvh5ycbf.1
Licensing provisions: CC BY 4.0
Programming language: C++
Nature of problem: Computing the Coulomb matrix elements (Coulomb and exchange integrals), while being a demanding computational task, is a necessary step in a range of quantum mechanical calculations. For example, in the field of nanostructures, such as quantum dots and nanowires or novel single dopant devices, this stage of calculation (even after a series of approximations) is at least an $O(N^2)$ operation (a summation over all pairs of N atoms or grid points in the analyzed system). Moreover, calculating the full Coulomb matrix usually requires the computation of thousands of such elements, thus presenting a formidable computational challenge.
Solution method: We provide a ready-to-use implementation for calculating Coulomb matrix elements for a given set of input wavefunctions in LCAO (linear combination of atomic orbitals) form resulting from tight-binding calculation. This implementation is based on the approach introduced in [1,2], by using a fast Fourier transform. In this work, we further significantly improved the method by eliminating the need to introduce wave-function transfer via auxiliary basis set.
Additional comments including Restrictions and Unusual features: The implementation is fully parallelized in a distributed-memory model, using MPI and parallel routines from FFTW [3].

References

[1] P.T. Różański, M. Zieliński, Linear scaling approach for atomistic calculation of excitonic properties of 10-million-atom nanostructures, Phys. Rev. B 94 (2016) 045440.
[2] P.T. Różański, M. Zieliński, Efficient computation of Coulomb and exchange integrals for multi-million atom nanostructures, Comput. Phys. Commun. (2019) 254.

☆ The review of this paper was arranged by Prof. Volker Blum.
☆☆ This paper and its associated computer program are available via the Computer Physics Communications homepage on ScienceDirect (http://www.sciencedirect.com/science/journal/00104655).

* Corresponding author.
E-mail address: rozanski@fizyka.umk.pl (P.T. Różański).

https://doi.org/10.1016/j.cpc.2023.108693

[3] M. Frigo, Steven G. Johnson, The design and implementation of FFTW3, Proc. IEEE 93 (2) (2005) 216–231, Invited paper, Special Issue on Program Generation, Optimization, and Platform Adaptation.

1. Introduction

Atomistic [1–9] approaches are state-of-the-art methods for modeling electronic and optical spectra of nanostructures, including various types of quantum dots and nanowires [10–20]. However, since atomistic approaches define systems in an atom-by-atom fashion, this leads to significant computational challenges, as often the number of atoms can easily exceed a million [21,19,9]. Computations for such systems are a formidable challenge in particular at the stage of the many-body part of the calculations, where interactions—Coulomb matrix elements—between single (quasi-)particles need to be accounted for.

For example, in the case of the empirical tight-binding (TB) methods where a linear combination of atomic orbitals (LCAO) is used, the straightforward calculation of Coulomb matrix elements would lead to a very unfavorable scaling of $O(N^4)$, where N is a number of atoms, which after a series of approximations this can be reduced to a quadratic-like $O(N^2)$ scaling [9]. Such $O(N^2)$ scaling, whereas acceptable for small systems (such as a $\sim$1 thousand atoms nanocrystal), is impractical for cases involving more than over a million of atoms (e.g. nanowire quantum dots) leading to an increase of the computational time by six orders of magnitude, as compared to 1 thousand atoms.

In our recent works [9,22] we have presented a solution to this problem. After a single particle stage of the calculation using the empirical tight binding method, we convert the LCAO wave-functions to a three-dimensional grid (with at most 30 grid points per atom) to obtain converged many-body spectra. This transfer from LCAO to a relatively coarse grid allows for the utilization of Fourier space methods on a grid namely the fast Fourier transform (FFT). The time of many-body calculation of Coulomb matrix elements scales as $O(N \log N)$, where N is the number of grid points linearly related to the number of atoms, and thus leading to a quasi-linear scaling in terms of the number of atoms. We have also presented a user-ready computer code-named Coulombo that is able to perform such quasi-linear (in time and memory) calculations of Coulomb and exchange integrals from real or complex wave-functions defined on a spatial, three-dimensional grid. The code also uses a zero-padding technique to avoid spurious interaction of charges from a super-cell with their periodic copies from other cells [23–25], and a graph-based algorithm for an efficient treatment of multiple integral calculations.

Here, we propose a new version of Coulombo code, named Coulomb-Lattice that omits conversion of the LCAO wave-function to an auxiliary grid altogether. In the previous version, such conversion has been performed by using some auxiliary (ad-hoc) basis set that is not only ambiguous, but may lead to strong basis dependence of final spectra [9]. The new Coulombo-Lattice code presented here exploits properties of the underlying crystal lattice, such a diamond, zinc-blende, wurtzite or lattice-mixed systems, where the regular, cubic grid of smaller lattice constants can be superimposed on a larger lattice constant grid of higher complexity. This is achieved automatically, by the program, by finding a regular superset of all possible atom positions. This idea, which is further elaborated in the text, allows Coulombo-Lattice to avoid the necessity of introducing an auxiliary basis set. The wave-function is transferred to a potentially much finer grid, maintaining all the advantages of the previous version including quasi-linear scaling computational time, removal of spurious interactions due to periodicity, and elasticity of user-provided screening model.

2. Problem description

In any given base of single-particle states ψ_n, the Coulomb matrix elements (elements of the matrix representation of the Coulomb operator) are defined as [26,6]

$$E_{ijkl} = \int \frac{\psi_i^*(\vec{r}_1)\psi_j^*(\vec{r}_2)\psi_k(\vec{r}_2)\psi_l(\vec{r}_1)}{\epsilon(\vec{r}_1-\vec{r}_2)|\vec{r}_1-\vec{r}_2|}\, dr_1^3\, dr_2^3\,, \tag{1}$$

where i, j, k and l are indices of single-particle functions, $\vec{r}_1$ and $\vec{r}_2$ span the entire computational domain, and ϵ stands for a position (distance) dependent dielectric function, which, in the simplest approximation, can often be replaced by a static dielectric constant.

In Ref. [9,22] we have shown that if the wave-functions are represented on a regular (but not necessarily equidistant) three-dimensional grid, these integrals can be computed effectively in quasi-linear time complexity depending on the size of the computational domain.

More specifically, introducing a regular with the grid steps of h_x, h_y and h_z, respectively, we can rewrite (1) as

$$E_{ijkl} = \sum_{\vec{r}_1}\sum_{\vec{r}_2} \rho_{il}(\vec{r}_1)\, G(\vec{r}_1-\vec{r}_2)\, \rho_{jk}(\vec{r}_2)\, h_x^2 h_y^2 h_z^2 \tag{2}$$

where $\rho_{il} = \psi_i^*\psi_l$ and $\rho_{jk} = \psi_j^*\psi_k$ are two "quasi-densities" formed by pairs of wavefunction and "interaction function" $G(\Delta r) = (\epsilon_0\epsilon(\Delta r)|\Delta r|)^{-1}$ depending on the precise model for dielectric function ϵ (assuming it depends on the distance only).

As a next step, we introduce the "quasi-potential" V_{jk} generated by one of the quasi-densities ρ_{jk}, which allows us to rearrange the equation as

$$E_{ijkl} = \sum_{\vec{r}_1} \rho_{il}(\vec{r}_1)\, V_{jk}(\vec{r}_1)\, h_x^2 h_y^2 h_z^2 \tag{3}$$

with V_{jk} defined as

$$V_{jk}(\vec{r}_1) = \sum_{\vec{r}_2} G(\vec{r}_1-\vec{r}_2)\, \rho_{jk}(\vec{r}_2) \tag{4}$$

which, in turn, can be rewritten as $V_{jk} = G \otimes \rho_{jk}$ where $\otimes$ denotes the full (non-periodic) convolution. Using the convolution theorem and either zero-padding or manipulating halves of the computational domain [22], this can be computed in quasi-linear $O(N \log N)$ time, where N is the number of grid points, linearly dependent on the number of atoms [9].

However, the solution described above requires the introduction of an auxiliary basis (e.g. Slater orbitals) in order to transform the results of TB calculations (i.e. wave-functions in LCAO form) to values on a regular three-dimensional grid. This additional step has a significant effect on results, especially in the case of exchange integrals, as they are apparently more prone to the non-orthogonality of the basis orbitals on the scale of the unit cell (as shown in [9]; see Fig. 5 in the referenced work and discussion that follows).

Moreover, the introduction of an arbitrary grid itself can affect the results, which may strongly depend on the precise value of the (somewhat arbitrary) grid step, and the obtained values of Coulomb and exchange integrals tend to oscillate even for seemingly fine grid steps. The comprehensive study of this effect is given in [9], in particular in Fig. 3 and Fig. 4.

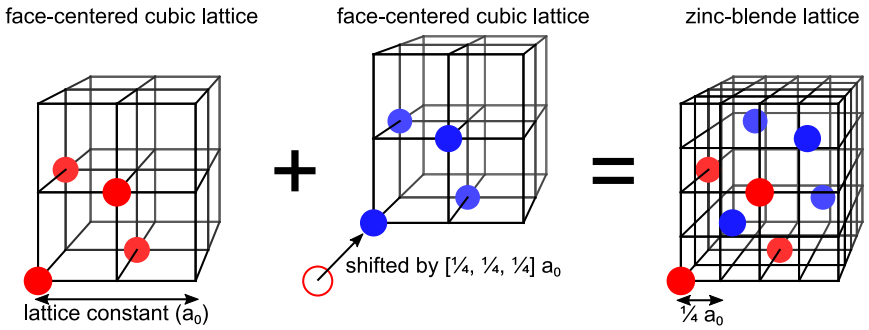

Fig. 1. Schematics illustrating that zinc-blende lattice can superimpose on a regular (cubic) grid with $\frac{1}{4}a_0$ lattice constant. The identical principle applies to silicon (diamond) lattice for the dopant problem studied in the text.

3. Introducing the intrinsic grid

Our solution is based on two remarks.

Firstly, for a wide class of regular atom arrangements (e.g. crystals) it is possible to define a regular three-dimensional grid as a superset of all possible atom positions. Such a construction for zinc-blende crystal, using a grid step of $0.25a_0$ (a_0 being the lattice constant) is shown on Fig. 1, thus effectively correspondingly to a regular lattice superimposed on crystal of lower-symmetry. Importantly such approach can be utilized for more complicated crystal lattices such as e.g. perovskites, quasi-two dimensional systems such as multi-layer transition-metal dichalcogenides (TMDC) systems, or even mixed-lattice systems as discussed later in the text. Importantly, this step of finding the optimal, regular, but not necessarily equidistant lattice is performed automatically by the program itself, by building a superset of atomic position read from the user provided file (in a simple, human readable format). More specifically, the algorithm builds a list of all displacements $\vec{r}_i - \vec{r}_0$ between positions of all atoms and the position of one, arbitrarily selected atom. Then, for each dimension separately, it calculates a greatest common divisor of all displacements using a floating-point version of the Euclidean algorithm. The obtained values for all three dimensions define the common grid. It can be shown that the resulting grid step does not depend on which atom's position is chosen as $\vec{r}_0$. The algorithm includes a sanity check for cases with no common grid step (e.g. due to significant strain in the system).

Secondly, the previously proposed efficient method of integral calculations is not based directly on the representation of wave-functions ψ_i, but rather on the quasi-densities $\rho_{jk} = \psi_j^* \psi_k$ and $\rho_{il} = \psi_i^* \psi_l$ formed as the scalar products of the wave-functions. Therefore, as long as the quasi-densities are represented as scalar fields, the wave-functions may have any generic representation, including the LCAO form specific for TB calculations. Thus, for simplicity, Coulombo-Lattice reads TB wave functions from user provided files given in a simple, human readable format. For user convenience, a simple example (including lattice file and wave functions) is provided together with the source code.

4. Comparison with $O(N^2)$ approach

For completeness, we briefly discuss here $O(N^2)$ method that is customarily [6,27,9] used for nanostructure calculations using the TB basis. We assume the TB wave function given as LCAO:

$$\psi_i = \sum_{\vec{R},\alpha} c^i_{\vec{R}\alpha} |\vec{R}\alpha\rangle, \tag{5}$$

where $\vec{R}\alpha$ is the α orbital localized on atom $\vec{R}$, and $c^i_{\vec{R}\alpha}$ is the LCAO expansion coefficient. By substituting Eq. (5) into Eq. (1) and then by utilizing a series of approximations i.e. neglecting four and three-center contributions, neglecting off-site exchange integrals due to the orthogonality and the localization of the atomic orbitals, and retaining only monopole-monopole terms in the multipole expansion of Coulomb (with more detail to be found in the Appendix A of Ref. [27] and in Ref. [6]), one gets an approximate form of Coulomb matrix elements:

$$\begin{aligned} E_{ijkl} = &\sum_{\vec{R}_1} \sum_{\vec{R}_2 \neq \vec{R}_1} \frac{e^2 \rho_{il} \rho_{jk}}{\epsilon \left| \vec{R}_1 - \vec{R}_2 \right|} \\ &+ \sum_{\vec{R}} \sum_{\alpha_1\alpha_2\alpha_3\alpha_4} c^{i*}_{\vec{R}\alpha_1} c^{j*}_{\vec{R}\alpha_2} c^{k}_{\vec{R}\alpha_3} c^{l}_{\vec{R}\alpha_4} U_{ijkl} \end{aligned} \tag{6}$$

where α is the orbital index and $\vec{R}_i$ denotes the position of the ith atom, ϵ is the dielectric constant corresponding to static screening used for simplicity, and $\rho_{il} = \sum_{\alpha_1} c^{i*}_{\vec{R}_1\alpha_1} c^{l}_{\vec{R}_1\alpha_1}$, $\rho_{jk} = \sum_{\alpha_2} c^{j*}_{\vec{R}_2\alpha_2} c^{k}_{\vec{R}_2\alpha_2}$ are quasi-densities calculated at each atomic site.

The first term is thus the long-range, bulk-screened, contribution to the two-center integral built from the monopole-monopole interaction [28,29] of two charge densities localized at different atomic sites. Due to the double summation, this part leads to unfavorable $O(N^2)$ scaling. The second term is the on-site unscreened part, with $U_{ijkl} = \langle \vec{R}_1\alpha_1, \vec{R}_1\alpha_2 \left| \frac{e^2}{|\vec{r}_1 - \vec{r}_2|} \right| \vec{R}_1\alpha_3, \vec{R}_1\alpha_4 \rangle$ are Coulomb matrix elements expressed in basis of atomic orbitals, typically calculated by direct integration using atomic (e.g. Slater) orbitals [30,31], however, it is often also estimated in a much simpler fashion by assuming a single U_0 onsite potential [27]. Either way, apart from the onsite term ambiguity, this part is much less computationally demanding—due to a single summation of all atoms it leads to $O(N)$ scaling—and is thus beyond the scope of this paper.

5. Results and benchmarks

5.1. P dopant in Si

We illustrate possible applications of the Coulombo-Lattice program, by running first calculations for a problem of single phosphorous dopant embedded and located at the center of a computationally tractable cubic block of the silicon host material, with several different box sizes used in the computation, as shown schematically in Fig. 2 (a).

Our calculation starts with the empirical TB calculation, with silicon TB parameters set taken from Ref. [32], the silicon block surface passivated by mimicking dangling bond passivation according to Ref. [33]. For the phosphorous dopant we use a dynamically-screened electrostatic potential $(\varepsilon(r)\, r)^{-1}$ with central-cell correction values tuned so the energy levels of the lowest six (twelve with spin) dopant bound states match the respective experimental values. The actual values of central-cell corrections depend

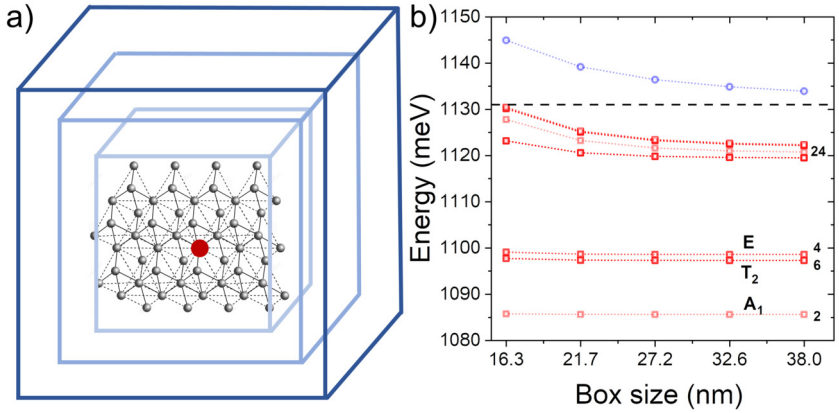

Fig. 2. (a) Schematics of P dopant (red dot) embedded in Si (black circles) host boxes of different dimensions, (b) Lowest 36 dopant levels as a function of the computational box size. Due to degeneracy (and near degeneracy) splittings of levels are practically not visible on the plot, hence number of levels (including spin) is shown on the right hand side. The black/dashed line marks the asymptotic bulk energy (1.131 eV) for Boykin et al. Si TB parameterization. The blue/dotted line corresponds to the ground state energy of an empty computational box. The ground-state (1s) manifold contains 6 (12 with spin) states named after their symmetry: A1 (two-fold with spin), T2 (six-fold with spin), and E (four-fold with spin). *(For interpretation of the colors in the figure(s), the reader is referred to the web version of this article.)*

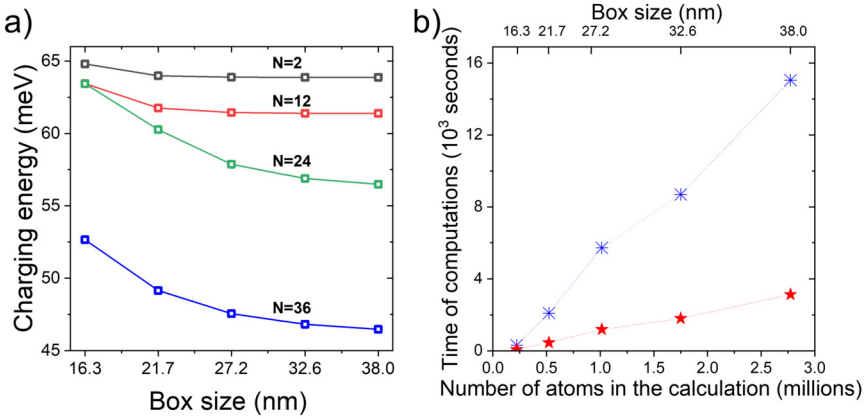

Fig. 3. (a) Dopant charging energy (see the text) calculated using CI method in the basis including the ground state only (2 states with spin), and with progressively large number of state including lowest 12 states, 24, and 36 states. (b) Time of computations of $36^4 \approx 1.68$ million Coulomb matrix elements (blue/dotted line) versus the size of computation box size/number of atoms. For comparison time of calculation using a smaller basis set ($24^4 \approx 0.332$) is shown (red/dashed line) again showing quasi-linear scaling.

strongly on the choice of dynamical screening parameters [34]. The actual dopant model and other details of TB calculations were discussed thoroughly in our recent work [35].

The results of TB calculations are shown in Fig. 2 (b), revealing the spectrum of dopant states including lowest "1s" manifold of 6 states (12 with spin). The "1s" manifold is split by central-cell correction [34] forming a two-fold degenerate A1 ground state (of ≈ 1.0856 eV energy corresponding to -45.6 meV dopant binging enegy), as well as 4-fold degenerate T2 and 2-fold degenerate E states (T2 ≈ 1.0973 eV, E ≈ 1.0986 eV). Higher dopant states (24 with spin) are also present, consistent with findings of other authors [36].

Here—at the TB states—we are limited by our SLEPc/PETSc TB eigensolver which takes about two days (on a 128-core machine) to resolve lowest 36 states for the largest computational box, and fails to converge for larger boxes, and even larger number of states, within a reasonable computational time. Nonetheless, we must emphasize here that TB part of computation has only auxiliary character for the current work.

Thus next, for TB/LCAO wave-functions we run the calculation of Coulomb matrix elements, which is of the essence for this work, and demonstrate that the resulting time and number of atoms shown in Fig. 3 (b) reveal quasi-linear scaling. We note here that the cost of computations (on the same machine), by using the direct, real space summation of Eq. (6) for the smallest considered box (0.22 million atoms), could be estimated to be 350× longer (by means of $O(N^2)$ scaling) than with Coulombo-Lattice, and it is estimated to be at least 50.000 times longer using Eq. (6) for the largest considered box (2.8 million atoms), thus leading to entirely prohibitive times of computations.

Following the definition from Ref. [36], the charging energy is calculated based on the two-electron ground state ($D^{-}_{\text{GS-FCI}}$) obtained by configuration interaction calculations, and the single-electron ground state (of a neutral dopant) from tight-binding simulations ($D^{0}_{\text{GS-TB}}$) as

$$D^{-}_{\text{CE}} = D^{-}_{\text{GS-FCI}} - 2D^{0}_{\text{GS-TB}}\,. \tag{7}$$

The utilization of several computational boxes of progressively larger dimensions is typically essential for the understanding of the convergence of single-particle and many-body properties for different nanostructures [37]. This is again pronounced in Fig. 3 (a) which shows results of the configurations interaction (CI) method calculation using Coulomb matrix elements calculated with Coulombo-Lattice. The CI method [38] has been widely used in quantum chemistry and physics. Details of the CI computations presented here are given e.g. in our earlier work [6]. CI results were obtained with different levels of approximation, i.e. by increasing the number of dopant levels used in the computation. Notably, the number (and cost of calculation) of Coulomb matrix

element scales with the fourth power of N, i.e. N^4, leading to a total of $36^4 \approx 1.68$ million, for $N = 36$, which for boxes with number of atoms up to 2.8 million is a computationally challenging task. Again we reiterate that we are limited by our SLEPc/PETSc TB eigensolver to resolve lowest 36 states for the largest computational box.

Both such a large basis of states, and a large number of atoms in the simulation are essential, since including only the ground dopant level would lead to a strong overestimation of dopant charging energy with its magnitude of approximately 65 meV, the inclusion of the lowest ("1s") dopant manifold 6 states (12 with spin), has relative small effect on the charging energy, whereas the inclusion of higher dopant states manifold notably reduces the binding energy to 46.8 meV, for the larger considered box, which can be further extrapolated to 46.2 meV for an asymptotic case (corresponding to the infinite box). This result is both quantitatively and qualitatively consistent with the results of Ref. [36] where the charging energy of ≈46 meV is reported by the incorporation of dopant shells higher than 1s.

Finally, we note here we used that we used $U_0 = 5$ eV for the modeling of the onsite part of the Coulomb interaction. However the final result is to a large degree immune to the actual choice of U_0, e.g. we obtained 47.1 meV charging energy for $U_0 = 10$ eV, N=36 and box of 2.8 million atoms. This can be (at least qualitatively) inferred from Fig. 3. The dopant wave functions are spatially distributed over thousands of atoms, and the charging energies are calculated in the basis of these functions. If we call this number M (not to be confused with the total number of atoms in the box N as $M \ll N$) there are still $O(M^2)$ long-range terms, and $O(M)$ short-range terms that depend on U_0. Although $M < N$, yet since M is still substantial, on the order of thousands (and M^2 millions), thus the integrals determining the charging energies are dominated by long-range contributions and not U_0 itself.

Our results indicate that atomistic linear scaling computations can be performed for novel atom-scale quantum devices utilizing precise dopant placement in Si for use in quantum computing [39] and analog quantum simulation [40]. Modeling a multi-dopant system is essential for understanding the connection between device performance and dopant arrangement [35], with more atomistic research likely to follow.

5.2. Crystal phase quantum dots

Crystal phase quantum dots [18] are formed during the nanowire vapor-liquid-solid (VLS) growth [41], by vertically stacking distinct crystal phases of the same chemical compound. One possible type of system is obtained by effectively sandwiching a thin zinc-blende layer between wurtzite phases (top row in Fig. 4). Due to different bandstructures of crystal phases [42], such systems are capable of binding excitons (interacting electron-hole pairs) and excitonic complexes [19]. Despite ZB section being only several lattice constant thin in the growth direction, the host nanowire usually has a large diameter (up to 70 nm) [19], and a substantial section of wurtzite needs to be accounted for converged spectra [37], as hole states tend to strongly localized in the WZ fragment [43]. All in all this leads to computational domains with a number of atoms regularly exceeding one million, making the state of single particle calculations challenging [9,43], and rendering the calculation of electron-hole Coulomb and exchange integrals with $O(N^2)$ method likely impractical.

As crystal phase quantum dots effectively consist of a mix of different crystal lattices, Coulombo-Lattice may not seem as a viable solution to the problem, However, as illustrated in Fig. 4 (two bottom rows) a common grid can be superimposed on both lattices. The grid is a rectangular grid with $1 : \sqrt{2} : \sqrt{6}$ ratios of grid steps in x, y, and z directions respectively. Again, we emphasize

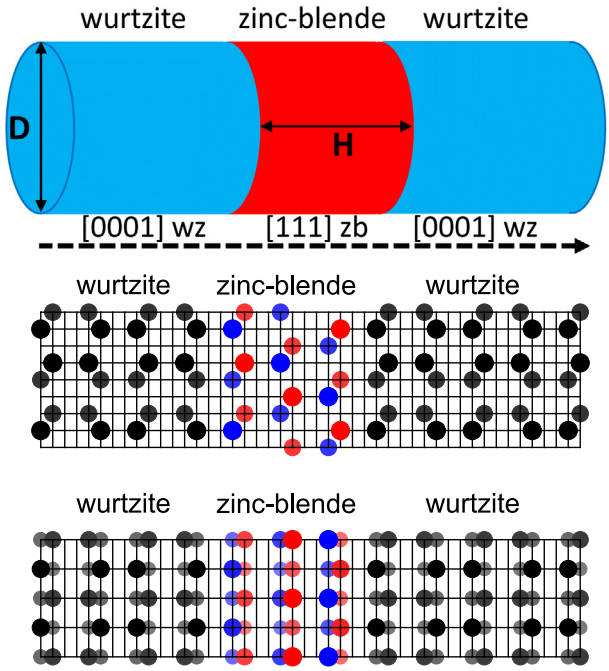

Fig. 4. Schematics showing (top row) [111] zinc-blende section embedded into wurtzite [0001] oriented nanowire. The dashed arrow shows the growth direction. The microscopic view (middle and bottom rows) shows that a common rectangular grid can be superimposed on a crystal phase quantum dot (see text for more details). The intrinsic grid for the zinc-blende/wurtzite/zinc-blende junction, as shown in two different planes. The step values of the common grid for this system are related to each other in proportions of $1 : \sqrt{2} : \sqrt{6}$.

that Coulombo-Lattice find such a grid in an automated way. The resulting grid is then fully suitable for FFT calculation performed by the rest of the code.

To illustrate the results of our calculations Fig. 5 (a) shows the evolution of excitonic ground state energy and associated excitonic binding energy (inset) calculated for an InP crystal phase quantum dot with a height of approximately 3 nm (three ABC stacking sequences). Fig. 5 (a) shows the typical reduction of excitonic energy with increasing system diameter (decreasing confinement). The corresponding binding energy (calculated as the energy difference between excitonic ground states and a single-particle gap) is shown in the inset.

These excitonic properties have been obtained for electron and hole found in the tight-binding self-consistent calculations (SCF), with details of calculation discussed in our recent works [43,44]. The CI part has been performed on top of SCF states using excitonic Hamiltonian as described in Ref. [6], and discussed by many other authors as well (e.g. Ref. [45]). In the CI calculation, we accounted for 3 lowest (6 with spin) electron states, and 4 lowest (8 with spin) hole states. This led to the calculation of a total of 10000 ($6^4 + 2 \times 6^2 \times 8^2 + 8^4$) various electron-electron, electron-hole, and hole-hole Coulomb and exchange matrix elements. The corresponding time of computation is shown on Fig. 5 (b). The time of computation again shows quasi-linear scaling with a number of atoms reaching 3.7 million (corresponding to a CPQD diameter of over 47 nm). Moreover, even for the largest considered systems, the time of computation is on a scale of several minutes only. This calculation was performed on a server with two 32-core AMD EPYC 7542 CPUs, with hyper-threading active (a total of 128 cores). The usage of Coulomb-Lattice thus reduced significantly the part of the calculation which up to now has been the most demanding computationally, to mere minutes, and the calculation is now dominated by the SCF/TB part of the computations which can be on a scale of days for the same computer.

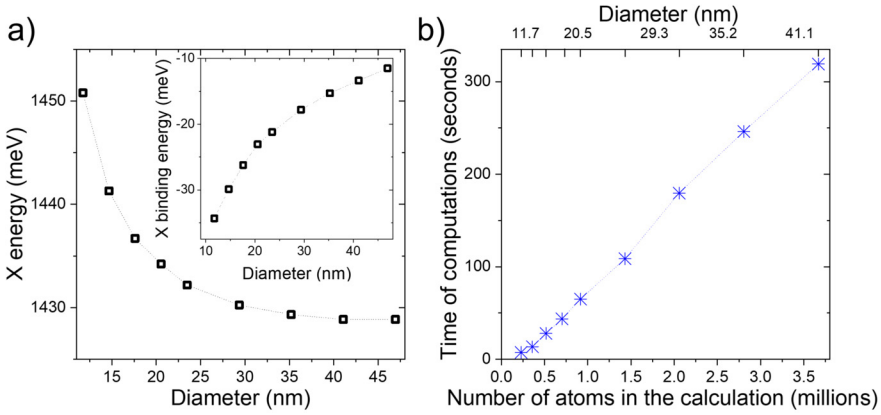

Fig. 5. (a) Exciton ground state energy calculated using Coulomb matrix elements computed by the Coulombo-Lattice program discussed in this work. The inset shows the corresponding excitonic binding energy. Both plots reveal the typical decrease of (absolute) magnitude with the increasing system diameter, and thus decreasing confinement. (b) The corresponding time of computation of Coulomb matrix elements (see text). Please note quadratic dependence between crystal phase quantum dot diameter and number of atoms in the system.

Table 1
Comparison of results, for several important Coulomb matrix elements, obtained by Coulomb-Lattice and the direct summation $O(N^2)$ for an imperfect lattice (approximately 3% strained and 50% alloyed) InGaAs self-assembled quantum dot with 0.56 million atoms. The comparison includes long-range parts only. The time of computation involves all Coulomb matrix elements in a basis of e_1, e_2, h_1 and h_2 states. Indices label (quasi)spins. The time of computation does not account for I/O operations (e.g. reading wave-functions).

	Coulombo-Lattice	$O(N^2)$	Relative error (%)
$\langle e_1 e_1 e_1 e_1 \rangle$ (meV)	22.21	21.97	1.1%
$\langle e_1 h_1 h_1 e_1 \rangle$ (meV)	22.00	21.77	1.05%
$\langle h_1 h_1 h_1 h_1 \rangle$ (meV)	22.31	22.09	1%
$\lvert\langle e_1 h_1 e_1 h_1 \rangle\rvert$ (μeV)	109.3	107.5	1.7%
$\lvert\langle e_1 h_2 e_2 h_1 \rangle\rvert$ (μeV)	1.87	1.83	2.2%
Time (s)	1.122	497.098	

5.3. Alloyed InGaAs quantum dot

We must note that the strain effects—that would deform ideal crystal lattice at ZB/WZ junction—are typically neglected or assumed to be very low («1%) in crystal-phase quantum dots [46–48, 43], thus strain should not be a major obstacle in using Coulombo-Lattice for weakly strained systems. However, a different scenario may occur for e.g. self-assembled quantum dots, the growth of which and properties of which are mainly driven by strain. Although Colombo-Lattice is not designed for these sort of systems, we can expect it to work at least in an approximated, yet satisfactory fashion. This can be done, for example, by feeding the program with TB wave-function obtained in presence of strain (non-perfect crystal lattice), yet assuming a perfect lattice for Coulomb matrix elements calculations. To illustrate this idea we have performed such calculation for, not only strained, but also alloyed InGaAs lens-shaped quantum dot located on a wetting layer, identical to one of random realizations of systems considered in Ref. [49].

Results shown in Table 1 indicate that Coulombo-Lattice can calculate Coulomb and exchange matrix elements for alloyed systems with relatively small error of up to several percent for the exchange integral ($\lvert\langle e_1 h_2 e_2 h_1 \rangle\rvert$) responsible for the bright exciton splitting [50], with even smaller ($\approx 1\%$) errors for electron-electron, electron-hole and electron-hole Coulomb integrals. If this level of error is acceptable, then Coulombo-Lattice provides—in this particular case—over 400× speedup as compared to straightforward $O(N^2)$ implementation running on the same machine. Further gains can be expected for using Coulomb-Lattice for calculations involving even larger number of electron and hole states.

Conclusions

We have presented a new version of efficient computer code aimed at quasi-linear scaling computation of Coulomb and exchange integrals for various nanostructures. The code named Coulomb-Lattice can be directly applied to a broad range of nanostructure, by exploiting the underlying crystal lattice. In this work, we have shown results of calculations for the nanostructures as distinct as crystal phases quantum dot (formed by interface of zinc-blende and wurtzite section of a nanowire) and systems composed of a single phosphorous dopant in silicon lattice, tackled by the same computational tool. Further applications to other widely researched nanostructures, such as perovskites or TMDCs are possible. Whereas our approach is designed for unstrained system, the program can still be used for non-perfect systems as well, assuming low strains, and if error bars up to several percent are acceptable.

The application of Coulombo-Lattice is attractive not only due to quasi-linear scaling, but also thanks to low absolute wall-clock time of calculations. The actual times are, on an example of a modern multi-core machine, ranging from individual seconds (for several integrals in a small quantum dot) up to only few hours (for 1.7 million integrals and 2.8 million atoms in the simulation).

Declaration of competing interest

The authors declare that they have no known competing financial interests or personal relationships that could have appeared to influence the work reported in this paper.

Data availability

The computer code is freely available in a Github repository (https://github.com/develancer/coulombo-lattice). Data for calculatons presented in this paper will be made available on request.

Acknowledgements

The authors would like to thank Garnett W. Bryant, Maicol A. Ochoa, and Martyna Patera for stimulating discussions and help in testing the software. The authors acknowledge support from the Polish National Science Centre based on decision No. 2015/18/E/ST3/00583.

References

[1] A.J. Williamson, L.W. Wang, A. Zunger, Phys. Rev. B 62 (2000) 12963–12977, https://doi.org/10.1103/PhysRevB.62.12963.
[2] G. Bester, S. Nair, A. Zunger, Phys. Rev. B 67 (2003) 161306, https://doi.org/10.1103/PhysRevB.67.161306.
[3] G. Klimeck, F. Oyafuso, T. Boykin, R. Bowen, P. von Allmen, Comput. Model. Eng. Sci. (CMES) 3 (2002) 601, https://engineering.purdue.edu/gekcogrp/publications/pubs_src/J_2002_1_freePU.pdf.
[4] F.A. Zwanenburg, A.S. Dzurak, A. Morello, M.Y. Simmons, L.C.L. Hollenberg, G. Klimeck, S. Rogge, S.N. Coppersmith, M.A. Eriksson, Rev. Mod. Phys. 85 (2013) 961–1019, https://doi.org/10.1103/RevModPhys.85.961.
[5] W. Jaskólski, M. Zieliński, G.W. Bryant, J. Aizpurua, Phys. Rev. B 74 (2006) 195339, https://doi.org/10.1103/PhysRevB.74.195339.
[6] M. Zieliński, M. Korkusinski, P. Hawrylak, Phys. Rev. B 81 (2010) 085301, https://doi.org/10.1103/PhysRevB.81.085301.
[7] M. Zieliński, Phys. Rev. B 86 (2012) 115424, https://doi.org/10.1103/PhysRevB.86.115424.
[8] G.W. Bryant, M. Zieliński, N. Malkova, J. Sims, W. Jaskólski, J. Aizpurua, Phys. Rev. B 84 (2011) 235412, https://doi.org/10.1103/PhysRevB.84.235412.
[9] P.T. Różański, M. Zieliński, Phys. Rev. B 94 (2016) 045440, https://doi.org/10.1103/PhysRevB.94.045440.
[10] G. Bester, A. Zunger, Phys. Rev. B 71 (2005) 045318, https://doi.org/10.1103/PhysRevB.71.045318.
[11] M. Zieliński, Nanoscale Res. Lett. 7 (1) (2012) 265, https://doi.org/10.1186/1556-276X-7-265.
[12] M. Zieliński, J. Phys. Condens. Matter 25 (46) (2013) 465301, http://stacks.iop.org/0953-8984/25/i=46/a=465301.
[13] M. Zieliński, Y. Don, D. Gershoni, Phys. Rev. B 91 (2015) 085403, https://doi.org/10.1103/PhysRevB.91.085403.
[14] R. Singh, G. Bester, Phys. Rev. B 84 (2011) 241402, https://doi.org/10.1103/PhysRevB.84.241402.
[15] R. Singh, G. Bester, Phys. Rev. Lett. 104 (2010) 196803, https://doi.org/10.1103/PhysRevLett.104.196803.
[16] M. Zieliński, K. Gołasa, M.R. Molas, M. Goryca, T. Kazimierczuk, T. Smoleński, A. Golnik, P. Kossacki, A.A.L. Nicolet, M. Potemski, Z.R. Wasilewski, A. Babiński, Phys. Rev. B 91 (2015) 085303, https://doi.org/10.1103/PhysRevB.91.085303.
[17] M. Zieliński, Phys. Rev. B 88 (2013) 155319, https://doi.org/10.1103/PhysRevB.88.155319.
[18] N. Akopian, G. Patriarche, L. Liu, J.-C. Harmand, V. Zwiller, Nano Lett. 10 (4) (2010) 1198–1201, https://doi.org/10.1021/nl903534n.
[19] M. Bouwes Bavinck, K.D. Jöns, M. Zieliński, G. Patriarche, J.-C. Harmand, N. Akopian, V. Zwiller, Nano Lett. 16 (2) (2016) 1081–1085, https://doi.org/10.1021/acs.nanolett.5b04217.
[20] M. Zieliński, Phys. Rev. B 88 (2013) 115424, https://doi.org/10.1103/PhysRevB.88.115424.
[21] M. Usman, J. Bocquel, J. Salfi, B. Voisin, A. Tankasala, R. Rahman, M.Y. Simmons, S. Rogge, L.C.L. Hollenberg, Nat. Nanotechnol. 11 (2016) 763.
[22] P.T. Różański, M. Zieliński, Comput. Phys. Commun. 238 (2019) 254–261, https://doi.org/10.1016/j.cpc.2018.12.011.
[23] G. Makov, M.C. Payne, Phys. Rev. B 51 (1995) 4014–4022, https://doi.org/10.1103/PhysRevB.51.4014.
[24] E.L. de Oliveira, E.L. Albuquerque, J.S. de Sousa, G.A. Farias, F.M. Peeters, J. Phys. Chem. C 116 (7) (2012) 4399–4407, https://doi.org/10.1021/jp2088516.
[25] A. Franceschetti, H. Fu, L.W. Wang, A. Zunger, Phys. Rev. B 60 (1999) 1819–1829, https://doi.org/10.1103/PhysRevB.60.1819.
[26] W. Sheng, S.-J. Cheng, P. Hawrylak, Phys. Rev. B 71 (2005) 035316, https://doi.org/10.1103/PhysRevB.71.035316.
[27] S. Schulz, S. Schumacher, G. Czycholl, Phys. Rev. B 73 (2006) 245327, https://doi.org/10.1103/PhysRevB.73.245327.
[28] A. Franceschetti, L.W. Wang, H. Fu, A. Zunger, Phys. Rev. B 58 (1998) R13367–R13370, https://doi.org/10.1103/PhysRevB.58.R13367.
[29] S.V. Goupalov, E.L. Ivchenko, Phys. Solid State 43 (10) (2001) 1867–1875, https://doi.org/10.1134/1.1410624.
[30] S. Lee, L. Jönsson, J.W. Wilkins, G.W. Bryant, G. Klimeck, Phys. Rev. B 63 (2001) 195318, https://doi.org/10.1103/PhysRevB.63.195318.
[31] K. Leung, K.B. Whaley, Phys. Rev. B 56 (1997) 7455–7468, https://doi.org/10.1103/PhysRevB.56.7455.
[32] T.B. Boykin, G. Klimeck, F. Oyafuso, Phys. Rev. B 69 (2004) 115201, https://doi.org/10.1103/PhysRevB.69.115201, https://link.aps.org/doi/10.1103/PhysRevB.69.115201.
[33] S. Lee, F. Oyafuso, P. von Allmen, G. Klimeck, Phys. Rev. B 69 (2004) 045316, https://doi.org/10.1103/PhysRevB.69.045316.
[34] M. Usman, R. Rahman, J. Salfi, J. Bocquel, B. Voisin, S. Rogge, G. Klimeck, L. Hollenberg, J. Phys. Condens. Matter 27 (15) (2015) 154207, https://doi.org/10.1088/0953-8984/27/15/154207.
[35] P.T. Różański, G.W. Bryant, M. Zieliński, npj Comput. Mater. 8 (1) (2022) 182, https://doi.org/10.1038/s41524-022-00857-w.
[36] A. Tankasala, J. Salfi, J. Bocquel, B. Voisin, M. Usman, G. Klimeck, M.Y. Simmons, L.C.L. Hollenberg, S. Rogge, R. Rahman, Phys. Rev. B 97 (2018) 195301, https://doi.org/10.1103/PhysRevB.97.195301, https://link.aps.org/doi/10.1103/PhysRevB.97.195301.
[37] M. Zieliński, Acta Phys. Pol. A 122 (2012) 312, http://przyrbwn.icm.edu.pl/APP/PDF/122/a122z2p15.pdf.
[38] A. Szabo, N. Ostlund, Modern Quantum Chemistry, MacMillan, 1983.
[39] Y. He, S.K. Gorman, D. Keith, L. Kranz, J.G. Keizer, M.Y. Simmons, Nature 571 (7765) (2019) 371–375, https://doi.org/10.1038/s41586-019-1381-2.
[40] X. Wang, E. Khatami, F. Fei, J. Wyrick, P. Namboodiri, R. Kashid, A.F. Rigosi, G. Bryant, R. Silver, Quantum simulation of an extended Fermi-Hubbard model using a 2D lattice of dopant-based quantum dots, arXiv:2110.08982, 2021.
[41] L.E. Jensen, M.T. Björk, S. Jeppesen, A.I. Persson, B.J. Ohlsson, L. Samuelson, Nano Lett. 4 (10) (2004) 1961–1964, https://doi.org/10.1021/nl048825k.
[42] A. De, C.E. Pryor, Phys. Rev. B 81 (2010) 155210, https://doi.org/10.1103/PhysRevB.81.155210.
[43] M. Patera, M. Zieliński, Phys. Rev. B 106 (2022) L041405, https://doi.org/10.1103/PhysRevB.106.L041405.
[44] M. Patera, M. Zieliński, Sci. Rep. 12 (2022) 15561, https://doi.org/10.1038/s41598-022-19076-w.
[45] P. Michler (Ed.), Topics in Applied Physics, vol. 90, Springer, New York, 2003.
[46] D. Kriegner, E. Wintersberger, K. Kawaguchi, J. Wallentin, M.T. Borgström, J. Stangl, Nanotechnology 22 (42) (2011) 425704, https://doi.org/10.1088/0957-4484/22/42/425704.
[47] L.C. Dacal, A. Cantarero, Solid State Commun. 151 (10) (2011) 781–784, https://doi.org/10.1016/j.ssc.2011.03.003, https://www.sciencedirect.com/science/article/abs/pii/S0038109811001232.
[48] P. Faria Junior, G. Sipahi, J. Appl. Phys. 112 (10) (2012) 103716, https://doi.org/10.1063/1.4767511, https://aip.scitation.org/doi/10.1063/1.4767511.
[49] M. Zieliński, Phys. Rev. B 103 (2021) 155418, https://doi.org/10.1103/PhysRevB.103.155418, https://link.aps.org/doi/10.1103/PhysRevB.103.155418.
[50] M. Bayer, O. Stern, A. Kuther, A. Forchel, Phys. Rev. B 61 (2000) 7273–7276, https://doi.org/10.1103/PhysRevB.61.7273.